Inorg. Chem. **2007**, *46*, 3585–3592

Solid-State ^{129}Xe and ^{131}Xe NMR Study of the Perxenate Anion XeO_6^{4-}

Michelle A. M. Forgeron,[†] Roderick E. Wasylishen,*[,†] Michael Gerken,[‡] and Gary J. Schrobilgen[§]

Department of Chemistry, Gunning/Lemieux Chemistry Centre, University of Alberta, Edmonton, Alberta T6G 2G2, Canada, Department of Chemistry and Biochemistry, University of Lethbridge, Lethbridge, Alberta T1K 3M4, Canada, and Department of Chemistry, McMaster University, Hamilton, Ontario L8S 4M1, Canada

Received December 21, 2006

Results of the first solid-state ^{131}Xe NMR study of xenon-containing compounds are presented. The two NMR-active isotopes of xenon, ^{129}Xe ($I = {}^1/_2$) and ^{131}Xe ($I = {}^3/_2$), are exploited to characterize the xenon magnetic shielding and quadrupolar interactions for two sodium perxenate salts, $Na_4XeO_6 \cdot xH_2O$ ($x = 0$, 2), at an applied magnetic field strength of 11.75 T. Solid-state $^{129/131}$Xe NMR line shapes indicate that the local xenon environment in anhydrous Na_4XeO_6 adopts octahedral symmetry, but upon hydration, the XeO_6^{4-} anion becomes noticeably distorted from octahedral symmetry. For stationary, anhydrous samples of Na_4XeO_6, the heteronuclear $^{129/131}$Xe–^{23}Na dipolar interaction is the principal contributor to the breadth of the $^{129/131}$Xe NMR lines. For stationary and slow magic-angle-spinning samples of $Na_4XeO_6 \cdot 2H_2O$, the anisotropic xenon shielding interaction dominates the ^{129}Xe NMR line shape, whereas the ^{131}Xe NMR line shape is completely dominated by the nuclear quadrupolar interaction. The xenon shielding tensor is approximately axially symmetric, with a skew of -0.7 ± 0.3, an isotropic xenon chemical shift of -725.6 ± 1.0 ppm, and a span of 95 ± 5 ppm. The ^{131}Xe quadrupolar coupling constant, 10.8 ± 0.5 MHz, is large for a nucleus at a site of approximate O_h symmetry, and the quadrupolar asymmetry parameter indicates a lack of axial symmetry. This study demonstrates the extreme sensitivity of the ^{131}Xe nuclear quadrupolar interaction to changes in the local xenon environment.

Introduction

The ability of noble gases to form compounds was first realized in 1962 when "$Xe^+PtF_6^-$" was reported.[1] Since then, other noble-gas compounds containing krypton[2] and xenon[3–5] have been synthesized in macroscopic amounts and radon chemistry has been explored by radiotracer techniques.[6] Most recently, an argon compound has been observed by low-temperature matrix-isolation techniques.[7] Of the noble gases, the chemistry of xenon is the most diverse,[4,5] and an extensive list of xenon(II), xenon(IV), xenon(VI), and xenon(VIII) compounds has been synthesized and characterized by solution NMR spectroscopy.[3] Recently, several transition metal–noble gas complexes have been synthesized where xenon is a ligand, e.g., $AuXe_4^{2+}$,[8] $Cr(CO)_5Xe$,[9] and (^{i}PrCp)-$Re(CO)(PF_3)Xe$.[10,11] A major limitation in high-oxidation-state xenon chemistry is that stable bonds with xenon are generally restricted to the most highly electronegative elements, namely, fluorine and oxygen, e.g., XeF_2, XeF_4, XeF_6, $XeOF_4$, XeO_2F_2, XeO_3, XeO_3F_2, XeO_4, and the perxenate anion, XeO_6^{4-}. Perxenate is among the most stable xenon species, which was first synthesized as the sodium salt by hydrolysis of XeF_6 in aqueous NaOH.[12,13] An

* To whom correspondence should be addressed. E-mail: roderick.wasylishen@ualberta.ca.
† University of Alberta.
‡ University of Lethbridge.
§ McMaster University.

(1) Bartlett, N. *Proc. Chem. Soc., London* **1962**, 218.
(2) Lehmann, J. F.; Mercier, H. P. A.; Schrobilgen, G. J. *Coord. Chem. Rev.* **2002**, *233–234*, 1–39.
(3) Gerken, M.; Schrobilgen, G. J. *Coord. Chem. Rev.* **2000**, *197*, 335–395.
(4) Holloway, J. H.; Hope, E. G. *Adv. Inorg. Chem.* **1998**, *46*, 51–100.
(5) Whalen, J. M.; Schrobilgen, G. J. In *Kirk–Othmer Encyclopedia of Chemical Technology*, 4th ed.; John Wiley & Sons, Inc.: New York, 1994; Chapter 13, pp 38–53.
(6) Fields, P. R.; Stein, L.; Zirin, M. H. *J. Am. Chem. Soc.* **1962**, *84*, 4164–4165.
(7) Khriachtchev, L.; Pettersson, M.; Runeberg, N.; Lundell, J.; Räsänen, M. *Nature* **2000**, *406*, 874–877.
(8) Seidel, S.; Seppelt, K. *Science* **2000**, *290*, 117–118.
(9) Simpson, M. B.; Polizkoff, M.; Turner, J. J.; Maier, W. B., II; McLaughlin, J. G. *J. Chem. Soc., Chem. Commun.* **1983**, 1355.
(10) Ball, G. E.; Darwish, T. A.; Geftakis, S.; George, M. W.; Lawes, D. J.; Portius, P.; Rourke, J. P. *Proc. Natl. Acad. Sci.* **2005**, *102*, 1853–1858.
(11) McMaster, J.; Portius, P.; Ball, G. E.; Rourke, J. P.; George, M. W. *Organometallics* **2006**, *25*, 5242–5248.

10.1021/ic0624524 CCC: $37.00
Published on Web 03/27/2007

improved synthesis employs the careful hydrolysis of XeF_6, followed by ozonation and basification of the resulting aqueous XeO_3 solution.[14] Perxenate exists in several salts having various degrees of hydration. The hydrates, $Na_4XeO_6 \cdot 8H_2O$,[15,16] $Na_4XeO_6 \cdot 6H_2O$,[17,18] and $K_4XeO_6 \cdot 9H_2O$,[19] have been unambiguously characterized by X-ray crystallography, while only unit cell parameters have been determined for $Na_4XeO_6 \cdot 2H_2O$[18,20] and Na_4XeO_6[20] by powder X-ray diffraction (XRD). Three potential $Na_4XeO_6 \cdot 2H_2O$ phases have been identified but none fully characterized,[20] and a single phase of anhydrous sodium perxenate has been reported.[20] The octahydrate, $Na_4XeO_6 \cdot 8H_2O$, was found to be more stable than $Na_4XeO_6 \cdot 6H_2O$, which readily decomposes to the dihydrate.[18] Anhydrous sodium perxenate can be obtained upon drying at 100 °C under dynamic vacuum.[21] Decomposition of sodium perxenate at 375 °C, accompanied by xenon loss, was observed.[22] Other perxenate salts that have been synthesized include those of cesium,[23] barium,[21,24] lanthanum,[24] and americium,[25] as well as $Na_3HXeO_6 \cdot H_2O$.[26]

Of the nine naturally occurring xenon isotopes, two are NMR-active, ^{129}Xe and ^{131}Xe. Owing to its high natural abundance (26.44%) and favorable nuclear properties ($I = {}^1/_2$, $\Xi = 27.810\,186$ MHz),[27] ^{129}Xe is the preferred isotope for NMR studies.[3,28] Nuclear magnetic resonance studies of the quadrupolar nuclide, ^{131}Xe ($I = {}^3/_2$; $\Xi = 8.243\,921$ MHz; $Q = -11.4$ fm^2; natural abundance, 21.18%),[27] are rendered more difficult by its relatively small nuclear magnetic moment, μ_N, and large nuclear quadrupole moment, Q. The small μ_N reduces the sensitivity of the NMR experiment, i.e., the Zeeman interaction, while the large Q causes exceedingly broad spectral lines in the solid state. Together, μ_N and Q make it intrinsically difficult to acquire ^{131}Xe NMR spectra of adequate signal-to-noise.

Although the direct observation of ^{129}Xe in chemically bound xenon species in the solid state is rare,[3,29,30] solution ^{129}Xe NMR studies are considerably more prevalent,[3,28] establishing a xenon chemical shift range of approximately 6500 ppm, where neat $XeOF_4$(l) at 24 °C is the accepted $^{129/131}$Xe NMR chemical shift reference.[3,27] Xenon chemical shifts depend on the formal oxidation state of xenon and qualitatively follow the trend $\delta(Xe^0) < \delta(Xe^{II}) < \delta(Xe^{IV}) < \delta(Xe^{VI})$.[3] The xenon chemical shift range was recently extended to approximately 7000 ppm upon measurement of the ^{129}Xe chemical shift of the xenon ligand in the organometallic transition-metal complex, $Re(^iPrCp)(CO)(PF_3)Xe$;[10] this complex represents the most shielded xenon species, $\delta_{iso} \approx -6179$ ppm, and is significantly more shielded than xenon gas.[3,28] Subsequent density functional theory calculations reproduce the experimental xenon chemical shift as well as the indirect spin−spin coupling constants $^2J(^{129}Xe-^{31}P)_{iso}$ and $^3J(^{129}Xe-^{19}F)_{iso}$.[11] The least shielded xenon species is XeO_2F^+ with a chemical shift of +704 ppm.[31] The originally reported chemical shift for XeO_6^{4-} in an aqueous solution, +2077 ppm,[31] is erroneous and has been corrected to −748 ppm.[3] The ^{129}Xe chemical shift has also been reported for solid, anhydrous sodium perxenate, ca. −720 ppm;[3] however, no information regarding the anisotropic interactions has been reported. Based on the assumption that the symmetry of the perxenate anion in the solid state is octahedral or that distortions from O_h symmetry are slight,[16,18,19] the anisotropic xenon shielding and quadrupolar interactions are expected to be small and measurable.

The most common ^{131}Xe NMR investigations involve atomic xenon because the ^{131}Xe quadrupolar coupling constants, C_Q, are generally small or zero. Most studies had focused on solutions of atomic xenon;[32] however, more recently, ^{131}Xe NMR spectroscopy of atomic xenon has been utilized to probe porous materials.[33−36] To date, only one solution ^{131}Xe NMR study of a molecular xenon-containing compound has been reported in which the ^{131}Xe chemical shifts of tetrahedral XeO_4 were measured in SO_2ClF, anhydrous HF, and BrF_5 solvents at −78.5, −75, and −50 °C, respectively.[37]

When examined independently, the two xenon isotopes, ^{129}Xe and ^{131}Xe, can provide complementary information: the ^{129}Xe nuclide probes the local xenon environment through characterization of the magnetic shielding interaction, while the quadrupolar ^{131}Xe nuclide probes the local and extended

(12) Malm, J. G.; Holt, B. D.; Bane, R. W. In *Noble-Gas Compounds*; Hyman, H. H., Ed.; University of Chicago Press: Chicago, 1963; Part 5, pp 167−173.
(13) Appelman, E. H. In *Noble-Gas Compounds*; Hyman, H. H., Ed.; University of Chicago Press: Chicago, 1963; Part 5, pp 185−190.
(14) Appelman, E. H. *Inorg. Synth.* **1968**, *11*, 210−213.
(15) Hamilton, W. C.; Ibers, J. A.; MacKenzie, D. R. *Science* **1963**, *141*, 532−534.
(16) Ibers, J. A.; Hamilton, W. C.; MacKenzie, D. R. *Inorg. Chem.* **1964**, *3*, 1412−1416.
(17) Zalkin, A.; Forrester, J. D.; Templeton, D. H.; Williamson, S. M.; Koch, C. W. *Science* **1963**, *142*, 501−502.
(18) Zalkin, A.; Forrester, J. D.; Templeton, D. H. *Inorg. Chem.* **1964**, *3*, 1417−1421.
(19) Zalkin, A.; Forrester, J. D.; Templeton, D. H.; Williamson, S. M.; Koch, C. W. *J. Am. Chem. Soc.* **1964**, *86*, 3569−3571.
(20) Hauck, J. *Z. Naturforsch., B: Chem. Sci.* **1970**, *25*, 226.
(21) Appelman, E. H.; Malm, J. G. *J. Am. Chem. Soc.* **1964**, *86*, 2141−2148.
(22) Mishin, V. Ya.; Kirin, I. S.; Isupov, V. K.; Gusev, Yu. K. *Russ. J. Inorg. Chem.* **1971**, *16*, 26; *Zh. Neorg. Khim.* **1971**, *16*, 51−55.
(23) Downey, G. D.; Claassen, H. H.; Appelman, E. H. *Inorg. Chem.* **1971**, *10*, 1817−1820.
(24) Shustov, L. D.; Tolmacheva, N. S.; Nabiev, Sh. Sh.; Il'in, E. K.; Klimov, V. D.; Ushakov, V. P. *Russ. J. Inorg. Chem.* **1989**, *34*, 946; *Zh. Neorg. Khim.* **1989**, *34*, 1673−1676.
(25) Marcus, Y.; Cohen, D. *Inorg. Chem.* **1966**, *5*, 1740−1743.
(26) Isupov, V. K.; Oleinik, A. V.; Aleinikov, N. N. *Russ. J. Inorg. Chem.* **1989**, *34*, 1183; *Zh. Neorg. Khim.* **1989**, *34*, 2080−2083.
(27) Harris, R. K.; Becker, E. D.; Cabral de Menezes, S. M.; Goodfellow, R.; Granger, P. *Pure Appl. Chem.* **2001**, *73*, 1795−1818.
(28) Schrobilgen, G. J. In *The Encyclopedia of Nuclear Magnetic Resonance*; Grant, D. M., Harris, R. K., Eds.; John Wiley and Sons: New York, 1996; Vol. 5, pp 3251−3262.
(29) Forgeron, M. A. M.; Wasylishen, R. E.; Penner, G. H. *J. Phys. Chem. A* **2004**, *108*, 4751−4758.
(30) Gerken, M.; Hazendonk, P.; Nieboer, J.; Schrobilgen, G. J. *J. Fluorine Chem.* **2004**, *125*, 1163−1168.
(31) Schrobilgen, G. J.; Holloway, J. H.; Granger, P.; Brevard, C. *Inorg. Chem.* **1978**, *17*, 980−987.
(32) Luhmer, M.; Reisse, J. *Prog. Nucl. Magn. Reson. Spectrosc.* **1998**, *33*, 57−76.
(33) Moudrakovski, I. L; Ratcliffe, C. I.; Ripmeester, J. A. *J. Am. Chem. Soc.* **2001**, *123*, 2066−2067.
(34) Meersmann, T.; Deschamps, M.; Bodenhausen, G. *J. Am. Chem. Soc.* **2001**, *123*, 941−945.
(35) Millot, Y.; Man, P. P.; Springuel-Huet, M.-A.; Fraissard, J. *C. R. Acad. Sci., Ser. IIc: Chim.* **2001**, *4*, 815−818.
(36) Clewett, C. F. M.; Pietrass, T. *J. Phys. Chem. B* **2005**, *109*, 17907−17912.
(37) Gerken, M.; Schrobilgen, G. J. *Inorg. Chem.* **2002**, *41*, 198−204.

xenon environment through measurement of the quadrupolar interaction. Thus, the relative sensitivities of the xenon shielding and quadrupolar interactions can be directly compared. For example, current literature reports[33−36] of xenon atoms trapped in well-defined sites in solids yield spans in the xenon shielding tensor ranging from 0 to 107 ppm[33] and $C_Q(^{131}Xe)$ values ranging from 0.28 to 6.47 MHz.[35] The large range of measured $C_Q(^{131}Xe)$ values demonstrates the sensitivity of the ^{131}Xe quadrupolar interaction relative to the anisotropic xenon shielding interaction. Results from a series of high-resolution microwave studies on small xenon-containing molecules[38−43] further emphasize the sensitivity of the ^{131}Xe quadrupolar interaction, with measured $C_Q(^{131}Xe)$ values ranging from +0.3875 MHz[38] for $^{131}Xe^{22}Ne$ to −369.50 MHz[39] for $^{131}Xe^{1}H^{+}$. To date, no solid-state ^{131}Xe NMR study of a xenon compound has been reported; however, such studies are expected to be severely hampered by the large ^{131}Xe nuclear quadrupole moment and the resulting large $C_Q(^{131}Xe)$ values.

In the present paper, two sodium perxenate salts, $Na_4XeO_6 \cdot xH_2O$ ($x = 0$, 2), have been investigated by solid-state ^{129}Xe and ^{131}Xe NMR spectroscopy at a moderate applied magnetic field strength (11.75 T). The two NMR-active isotopes of xenon, ^{129}Xe and ^{131}Xe, have been exploited to characterize the xenon magnetic shielding and electric field gradient (EFG) tensors, thus representing the first solid-state ^{131}Xe NMR studies of xenon compounds.

Results and Discussion

Background Theory. The important NMR interactions for xenon in $Na_4XeO_6 \cdot xH_2O$ ($x = 0$, 2) are the magnetic shielding (chemical shift) interaction, the nuclear quadrupolar interaction (for ^{131}Xe only), and the heteronuclear $^{129/131}Xe-^{23}Na$ dipolar interaction. The quadrupolar interaction is sensitive to small EFGs at the observed nucleus that depend on r_{ij}^{-3}, where r_{ij} is the distance between a particular charge, i, and the observed nucleus, j; thus, long-range effects may make important contributions to the EFG. An important distinction between the EFG and magnetic shielding interaction is that the EFG is a first-order property and depends only on the electronic ground state of the molecule,[44] whereas the magnetic shielding interaction is a second-order property that depends on excited electronic states. The following discussion is limited to definitions and discussion relevant to the work presented herein; detailed descriptions of the theories of nuclear magnetic shielding[45−49] and quadrupolar[50−53] interactions have been presented elsewhere.

In the solid state, three parameters are required to describe the symmetric part of the magnetic shielding tensor: the isotropic magnetic shielding, span, and skew.[54] Alternatively, one may define an anisotropy instead of a span and an asymmetry parameter instead of a skew.[55,56] Experimentally, the magnetic shielding at a nucleus is measured in terms of the chemical shift, δ, i.e., the difference in ppm between a sample peak and that of a standard reference peak; the isotropic value is given by $\delta_{iso}/\text{ppm} = [\nu(\text{sample})_{iso} - \nu(\text{ref})_{iso}]/\nu(\text{ref})_{iso}$. The breadth of the observed shielding values is described by the span, $\Omega = \delta_{11} - \delta_{33}$, and the line shape is described by the skew, $\kappa = 3(\delta_{22} - \delta_{iso})/\Omega$, which can take on values of −1 to +1, inclusive.[54] The principal components of the xenon chemical shift tensor are ordered such that $\delta_{11} \geq \delta_{22} \geq \delta_{33}$.

The quadrupolar interaction is generally the most important perturbation of the Zeeman interaction in solid-state NMR spectra of quadrupolar nuclei, i.e., those with a nuclear spin greater than $^1/_2$. The quadrupolar interaction[50−53] arises from the interaction of the nuclear electric quadrupole moment, eQ, with the EFG at the nucleus. The EFG is properly described by a symmetric, traceless second-rank tensor. In its principal-axis system, the EFG tensor is diagonal with $\sum_{\alpha\alpha} V_{\alpha\alpha} = 0$ and is characterized by two parameters: the largest principal component of the EFG tensor, V_{ZZ}, and the asymmetry parameter, $\eta_Q = (V_{XX} - V_{YY})/V_{ZZ}$, where $|V_{ZZ}| \geq |V_{YY}| \geq |V_{XX}|$. The nuclear quadrupolar coupling constant is a convenient measure of the strength of the quadrupolar interaction and may be expressed in frequency units by $C_Q = eQV_{ZZ}/h$, where h is Planck's constant.

Last, the dipolar interaction is a "through-space" interaction between two nuclear spins, N and N', and is analogous to the classical interaction between two bar magnets.[57] The strength of the dipolar interaction is measured in terms of

(38) Jäger, W.; Xu, Y.; Gerry, M. C. L. *J. Chem. Phys.* **1993**, *99*, 919−927.
(39) Peterson, K. A.; Petrmichl, R. H.; McClain, R. L.; Woods, R. C. *J. Chem. Phys.* **1991**, *95*, 2352−2360.
(40) Cooke, S. A.; Gerry, M. C. L. *Phys. Chem. Chem. Phys.* **2004**, *6*, 3248−3256.
(41) Keenan, M. R.; Buxton, L. W.; Campbell, E. J.; Balle, T. J.; Flygare, W. H. *J. Chem. Phys.* **1980**, *73*, 3523−3529.
(42) Baiocchi, F. A.; Dixon, T. A.; Joyner, C. H.; Klemperer, W. *J. Chem. Phys.* **1981**, *75*, 2041−2046.
(43) Cooke, S. A.; Gerry, M. C. L. *J. Am. Chem. Soc.* **2004**, *126*, 17000−17008.
(44) Wasylishen, R. E. W. In *Calculation of NMR and EPR Parameters: Theory and Applications*; Kaupp, M., Bühl, M., Malkin, V. G., Eds.; Wiley-VCH: Weinheim, Germany, 2004; Chapter 27, pp 433−447.
(45) Haeberlen, U. In *Advances in Magnetic Resonance*; Waugh, J. S., Ed.; Academic Press: New York, 1976; Suppl. 1, Vol. 6, Chapter III, pp 17−35.
(46) Anet, F. A. L.; O'Leary, D. J. *Concepts Magn. Reson.* **1991**, *3*, 193−214.
(47) Anet, F. A. L.; O'Leary, D. J. *Concepts Magn. Reson.* **1992**, *4*, 35−52.
(48) Veeman, W. S. *Prog. Nucl. Magn. Reson. Spectrosc.* **1984**, *16*, 193−235.
(49) Facelli, J. C.; Grant, D. M. *Top. Stereochem.* **1989**, *19*, 1−61.
(50) Samoson, A. *Chem. Phys. Lett.* **1985**, *119*, 29−32.
(51) Amoureux, J. P.; Fernandez, C.; Granger, P. In *Multinuclear Magnetic Resonance in Liquids and Solids—Chemical Applications, Series C: Mathematical and Physical Sciences*; Granger, P., Harris, R. K., Eds.; Kluwer Academic Publishers: Dordrecht, The Netherlands, 1990; Vol. 322, Chapter 22, pp 409−424.
(52) Abragam, A. In *Principles of Nuclear Magnetism*; Adair, R. K., Elliott, R. J., Marshall, W. C., Wilkinson, D. H., Eds.; Clarendon Press: Oxford, U.K., 1961; Chapter 7, pp 216−263.
(53) Duer, M. J.; Farnan, I. In *Solid-State NMR Spectroscopy: Principles and Applications*; Duer, M. J., Ed.; Blackwell Science: Oxford, U.K., 2002; Vol. 1, Chapter 4, pp 179−184.
(54) Mason, J. *Solid State Nucl. Magn. Reson.* **1993**, *2*, 285−288.
(55) Mehring, M. *Principles of High Resolution NMR in Solids*, 2nd ed.; Springer-Verlag: Berlin, 1983; Chapter 2, p 48.
(56) Spiess, H. W. In *NMR, Basic Principles and Progress*; Diehl, P., Fluck, E., Kosfeld, R., Eds.; Springer-Verlag: Berlin, 1978; Vol. 15, p 76.
(57) Wasylishen, R. E. In *Encyclopedia of Nuclear Magnetic Resonance*; Grant, D. M., Harris, R. K., Eds.; John Wiley & Sons: Chichester, U.K., 1996; Vol. 3, pp 1685−1695.

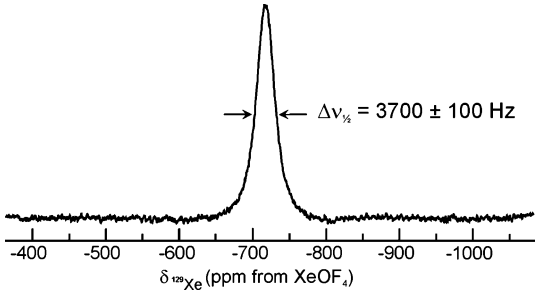

Figure 1. Experimental solid-state ^{129}Xe NMR spectrum of a stationary sample of anhydrous Na_4XeO_6 acquired at 139.0314 MHz (B_0 = 11.75 T) using a spin−echo sequence, a pulse delay of 2 s, and 1600 scans.

the dipolar coupling constant (in hertz),[57] $R_{DD} = (\mu_0/4\pi)(\hbar/2\pi)\gamma_N\gamma_{N'}r_{NN'}^{-3}$, where μ_0 is the vacuum permittivity, $\hbar$ is the reduced Planck's constant, $h/2\pi$, γ_N is the magnetogyric ratio of nucleus N, and $r_{NN'}$ is the internuclear N−N′ vector. Of the three aforementioned NMR interactions important for xenon in sodium perxenate, the $^{129/131}$Xe−^{23}Na dipolar interactions are expected to be the least important, with magnitudes on the order of 10^2 Hz. Note that $^{129/131}$Xe−^{17}O dipolar coupling is negligible because of the low natural abundance and small value of γ for ^{17}O.

Anhydrous Na_4XeO_6. (a) Solid-State ^{129}Xe NMR Spectroscopy. The ^{129}Xe NMR spectrum of a stationary Na_4XeO_6 sample is presented in Figure 1. The isotropic chemical shift of anhydrous Na_4XeO_6, −721 ± 1 ppm, is in good agreement with the previously reported value, −720 ± 1 ppm.[3] The line shape of the ^{129}Xe NMR peak shows no evidence of anisotropic xenon shielding, suggesting that the structure of the XeO_6^{4-} anion is a perfect octahedron,[58] as predicted by simple valence-shell electron-pair repulsion rules. Inspection of the ^{129}Xe NMR peak reveals that it has a Lorentzian shape, which is unusual in the solid state, where NMR line shapes are characteristically Gaussian.[59] Lorentzian line shapes are observed in solids when there is considerable motional averaging, as observed in solution NMR spectroscopy.[59] For the octahedral perxenate anion, it is likely that rapid jumps are occurring about the 2-, 3-, and 4-fold symmetry axes. Such motion is reasonable, particularly for anhydrous Na_4XeO_6, where the absence of water eliminates the possibility of hydrogen bonding and further supports the possibility of rapid reorientation of the XeO_6^{4-} anion. Other octahedral molecules and anions that exhibit rapid reorientational motion in the solid state are the neutral transition-metal hexafluorides (MF_6; M = Pu, W, Os, Pt, Mo)[60] and main-group hexafluoro anions (EF_6^-; E = P,[61,62] As,[63] Sb[62,63]).

The argument that the XeO_6^{4-} anion is rapidly jumping raises another question as to whether the anion truly possesses octahedral symmetry or whether the isotropic ^{129}Xe NMR line shape arises as a consequence of motional averaging of an anion distorted from O_h symmetry. Our solid-state ^{131}Xe NMR results and Raman spectroscopic data for anhydrous Na_4XeO_6 provide further conclusive evidence that xenon resides in a site of octahedral symmetry (vide infra).

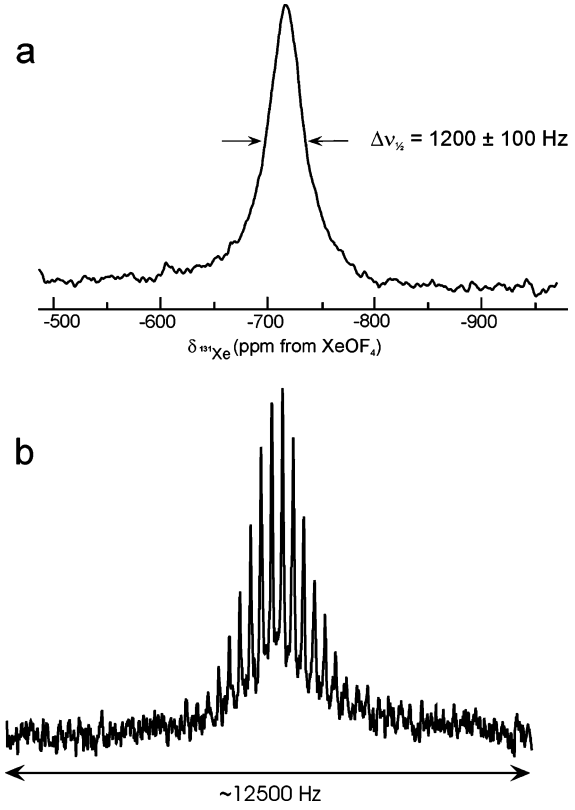

Figure 2. Solid-state ^{131}Xe NMR spectra of stationary samples of anhydrous Na_4XeO_6 acquired at 41.2136 MHz (B_0 = 11.75 T) using (a) spin−echo (52 432 scans) and (b) QCPMG (53 024 scans; ν_{QCPMG} = 200 Hz) experiments. An apodization function of 100 Hz was applied to the experimental spectrum (a) upon Fourier transformation.

The line width at half-height, $\Delta\nu_{1/2}$, of the ^{129}Xe NMR peak (Figure 1) is 3700 ± 100 Hz. The broadening must arise mainly from the heteronuclear ^{129}Xe−^{23}Na dipolar interaction because the anisotropic xenon shielding interaction is zero for octahedral site symmetry[58] and the indirect spin−spin, spin−rotation, paramagnetic, and quadrupolar interactions are irrelevant for ^{129}Xe in Na_4XeO_6. Unfortunately, the absence of an X-ray crystal structure for anhydrous Na_4XeO_6 precludes calculation of the dipolar coupling constant, R_{DD}(^{129}Xe,^{23}Na), and quantitative analysis of the dipolar interaction.

The ^{129}Xe spin−lattice relaxation time, T_1(^{129}Xe), was measured using the progressive saturation technique[64] and determined to be 90 ± 10 s, demonstrating that spin−lattice relaxation is inefficient for Na_4XeO_6.

(b) Solid-State ^{131}Xe NMR Spectroscopy. Solid-State ^{131}Xe NMR spectra of a stationary anhydrous sample of Na_4XeO_6, shown in Figure 2, are in accord with the ^{129}Xe NMR results in that an isotropic ^{131}Xe NMR line shape is observed. This result resolves the question regarding the

(58) Buckingham, A. D.; Malm, S. M. *Mol. Phys.* **1971**, *22*, 1127−1130.
(59) Fukushima, E.; Roeder, S. B. W. *Experimental Pulse NMR: A Nuts and Bolts Approach*; Addison-Wesley Publishing Co., Inc.: London, 1981; Chapter IV, Section A. 2, pp 227−241.
(60) Blinc, R.; Pirkmajer, E.; Slivnik, J.; Zupančič, I. *J. Chem. Phys.* **1966**, *45*, 1488−1495.
(61) Miller, G. R.; Gutowsky, H. S. *J. Chem. Phys.* **1963**, *39*, 1983−1994.
(62) Andrew, E. R.; Firth, M.; Jasinski, A.; Randall, P. J. *Phys. Lett.* **1970**, *31A*, 446−447.
(63) Andrew, E. R.; Farnell, L. F.; Gledhill, T. D. *Phys. Rev. Lett.* **1967**, *19*, 6−7.
(64) Freeman, R.; Hill, H. D. W. *J. Chem. Phys.* **1971**, *54*, 3367−3377.

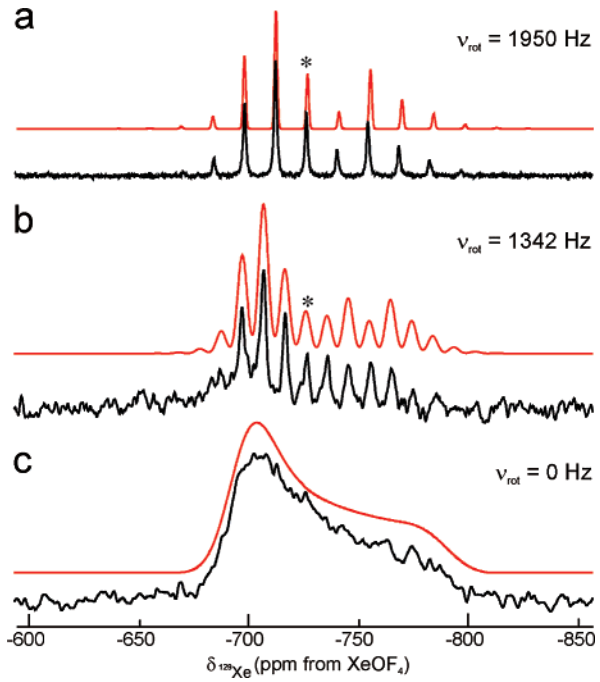

Figure 3. Simulated (top trace) and experimental (bottom trace) solid-state $^{129}Xe\{^1H\}$ NMR spectra of $Na_4XeO_6{\cdot}2H_2O$ acquired at 11.75 T using various spinning rates. Spectra shown were acquired using (a) CP/TPPM with a pulse delay of 2 s and are the sum of 4096 scans and (b and c) one-pulse experiments with a 30-s pulse delay and are the sum of 1916 (b) and 6516 (c) scans. Processing parameters for spectra (a−c) include line broadening (15, 150, and 300 Hz, respectively) and zero-filling (16, 4, and 8 K, respectively). Best-fit simulated xenon shielding parameters are given in Table 1.

local xenon environment in the XeO_6^{4-} anion. If the XeO_6^{4-} anion were slightly distorted from O_h symmetry, an EFG at xenon would result; this EFG would be amplified by the large nuclear quadrupole moment of ^{131}Xe and give rise to a broad ^{131}Xe NMR signal with a characteristic quadrupolar line shape. Rapid reorientation of the XeO_6^{4-} anion is ineffective in averaging this interaction; hence, the only logical explanation for the isotropic ^{129}Xe and ^{131}Xe NMR line shapes is that the xenon atom in anhydrous Na_4XeO_6 resides in a site of true octahedral symmetry. Raman spectroscopic data for anhydrous Na_4XeO_6 also support this conclusion. Three vibrational bands, consistent with O_h symmetry, were observed in the Raman spectrum and are assigned as follows (relative intensities are in parentheses): $\nu_1(A_{1g})$, 684 (100) cm^{-1}; $\nu_2(E_g)$, 654 (26) cm^{-1}; $\nu_5(T_{2g})$, 469 (16) cm^{-1}.

The line width of the ^{131}Xe NMR peak (1200 Hz) is significantly less than that of the ^{129}Xe NMR peak (3700 Hz). The ratio, $\Delta\nu_{1/2}(^{129}Xe)/\Delta\nu_{1/2}(^{131}Xe) = 3.1$, is approximately equal to the ratio of their respective resonance frequencies, $\Xi(^{129}Xe)/\Xi(^{131}Xe) = 3.4$, strongly supporting the contention that broadening of the ^{129}Xe and ^{131}Xe NMR peaks arises from $^{129/131}Xe-^{23}Na$ dipolar interactions. Because the dipolar interaction is directly related to the product of the magnetogyric ratios of the coupled spins, $\gamma^{129}_{Xe}\gamma^{23}_{Na}$ and $\gamma^{131}_{Xe}\gamma^{23}_{Na}$, a greater line width is expected for the ^{129}Xe NMR peak relative to that of its quadrupolar counterpart, ^{131}Xe.

The $T_1(^{131}Xe)$ for Na_4XeO_6 was not accurately determined but was estimated to be less than 1 s by monitoring the ^{131}Xe NMR peak intensity as a function of the pulse delay. The $T_2(^{131}Xe)$ value was sufficiently long, ~30 ms, to carry out a QCPMG experiment. The line widths of the spikelet sidebands in the QCPMG spectrum are dictated by the experimental digital resolution. In this case, the line widths, 35 ± 5 Hz, indicate that homogeneous interactions are small for anhydrous Na_4XeO_6.

$Na_4XeO_6{\cdot}2H_2O$. (a) Solid-State ^{129}Xe NMR Spectroscopy. Experimental and simulated solid-state $^{129}Xe\{^1H\}$ NMR spectra of $Na_4XeO_6{\cdot}2H_2O$ are shown in Figure 3, and the parameters, δ_{iso}, Ω, and κ, that provided the best fits for the simulated spectra are given in Table 1. The xenon shielding tensor is anisotropic, which immediately indicates deviation of the XeO_6^{4-} anion from O_h symmetry. The span of the xenon shielding tensor is small, 95 ± 5 ppm, relative to the xenon chemical shift range, ~7000 ppm, suggesting that distortion of the anion is small. The span also suggests the absence of rapid isotropic motion of the XeO_6^{4-} anion in $Na_4XeO_6{\cdot}2H_2O$. The water molecules likely restrict motion of the XeO_6^{4-} anion because of its lower site symmetry in the crystal lattice and hydrogen-bonding interactions with XeO_6^{4-}.

The isotropic ^{129}Xe chemical shift, −725.6 ± 1.0 ppm, is close to the previously published value for solid anhydrous perxenate, −721 ± 1 ppm.[3] The xenon shielding tensor is, within error limits, axially symmetric, $0.7 \leq \kappa \leq 1.0$, suggesting that a C_n axis ($n \geq 3$) may be present; however, the value of η_Q (vide infra) does not support axial symmetry. Unfortunately, determination of accurate δ_{ii} values for axially symmetric, or near axially symmetric, chemical shift tensors is a well-known problem for magic-angle-spinning (MAS) samples and precludes more accurate determination of κ.[65]

The $^{129}Xe\{^1H\}$ NMR spectra of both slow-spinning MAS samples and stationary samples of $Na_4XeO_6{\cdot}2H_2O$, shown in Figure 3, are broadened; the most plausible source of this broadening is $^{129}Xe-^{23}Na$ dipolar coupling, $R_{DD}(^{129}Xe,^{23}Na)$. An accurate value of $R_{DD}(^{129}Xe,^{23}Na)$, which depends explicitly on r_{XeNa}, cannot be calculated because the structure of $Na_4XeO_6{\cdot}2H_2O$ has not been determined. However, an estimate of R_{DD} may be obtained from the reported Na···Xe distances in the known single-crystal X-ray structures of $Na_4XeO_6{\cdot}8H_2O$[15,16] and $Na_4XeO_6{\cdot}6H_2O$.[17,18] The value thus obtained, ~235 Hz, is comparable to the line broadening that was applied to the simulated spectrum for the stationary sample, shown in Figure 3c. In addition, the ^{129}Xe NMR spectra of MAS samples shown in Figure 3a,b illustrate that, upon employment of faster MAS rates, the heteronuclear ^{129}Xe ^{23}Na interactions are more effectively averaged, as demonstrated by the reduction in the line width of the spinning sidebands from 400 ± 15 Hz at $\nu_{rot} = 1342$ Hz to 200 ± 10 Hz at $\nu_{rot} = 1950$ Hz.

In the absence of detailed structural data, it is instructive to investigate the $^1H \rightarrow {}^{129}Xe$ cross-polarization (CP) dynamics to estimate the strength of the $^1H-^{129}Xe$ dipolar

(65) Clayden, N. J.; Dobson, C. M.; Lian, L.-Y.; Smith, D. J. *J. Magn. Reson.* **1986**, *69*, 476−487.

Table 1. Experimental Xenon EFG and Shielding Parameters for $Na_4XeO_6 \cdot xH_2O$ ($x = 0$, 2) and Two Unknown Hydrates of Sodium Perxenate[a]

	δ_{iso}, ppm	C_Q, MHz	η_Q	Ω, ppm	κ
Na_4XeO_6	-721 ± 1				
$Na_4XeO_6 \cdot 2H_2O$	-725.6 ± 1.0	10.8 ± 0.5	0.48 ± 0.05	95 ± 5	$0.7 \leq \kappa \leq +1.0$
hydrate 1	-700 ± 1.0	3.5 ± 0.5	0.6 ± 0.1	*b*	*b*
hydrate 2	-743 ± 1.0	3.5 ± 0.5	0.6 ± 0.1	*b*	*b*

[a] The unknown hydrates may be polymorphic phases of $Na_4XeO_6 \cdot 2H_2O$ or other hydrate phases, i.e., $Na_4XeO_6 \cdot xH_2O$ ($x \neq 2$). [b] The anisotropic xenon shielding parameters for the unknown Na_4XeO_6 hydrates have not been determined but are believed to be negligible.

interaction and therefore the proximities of the water molecules. The CP parameters, $T_{^1H^{129}Xe}$ and $T_{1\rho}(^1H)$, have been determined by measuring the normalized ^{129}Xe NMR peak intensity as a function of the contact time, t_{CT}, for $Na_4XeO_6 \cdot 2H_2O$. Nonlinear regression analysis[66] of the characteristic "rise−fall" curve, fit to eq 1,[67] where I is the peak intensity and I_0 is a proportionality constant, yields values for $T_{^1H^{129}Xe}$ and $T_{1\rho}$ of 3.37 and 18.2 ms, respectively, with an estimated error of ±10%. Although $T_{^1H^{129}Xe}$ provides

$$I = \frac{I_0\{\exp[-t_{CT}/T_{1\rho}(^1H)] - \exp[-t_{CT}/T_{^1H^{129}Xe}]\}}{[1 - T_{^1H^{129}Xe}/T_{1\rho}(^1H)]} \quad (1)$$

valuable information about the general strength of the $^1H-^{129}Xe$ dipolar interaction, the individual $^1H\cdots^{129}Xe$ distances cannot be determined.

Upon variation of the contact time, two much smaller xenon peaks became visible in the ^{129}Xe NMR spectrum. One peak appeared at −743 ppm, to a slightly lower frequency of $\delta_{iso}(Xe)$ for the dihydrate, and became apparent with the use of a long contact time (20 ms), while the second peak appeared at −700 ppm, to a higher frequency of δ_{iso}(Xe), and was visible with the use of shorter contact times, ≤3 ms. Given their similar chemical shifts, it is reasonable to attribute these peaks to other sodium perxenate hydrates or to polymorphic phases of the dihydrate. The NMR peaks of the hydrate impurities became more pronounced using a one-pulse ^{129}Xe experiment with ^1H decoupling; however, relative to the main component, $Na_4XeO_6 \cdot 2H_2O$, their intensities are weak.

(b) Solid-State ^{131}Xe NMR Spectroscopy. The ^{131}Xe QCPMG spectra of $Na_4XeO_6 \cdot 2H_2O$ acquired at 11.75 T using the stepped-frequency technique are shown in Figure 4. Selected subspectra are shown in Figure 4a, and the complete ^{131}Xe NMR spectrum, processed using the skyline projection method,[68] is shown in Figure 4b. The spectrum spans ca. 500 kHz and was acquired over a period of 25 days. While the signal-to-noise ratio of the spectrum is poor, it is sufficient to estimate a $C_Q(^{131}Xe)$ value of ca. 11 MHz. Deviation of the XeO_6^{4-} anion from ideal O_h symmetry is apparent from the large $C_Q(^{131}Xe)$ value and is in agreement with ^{129}Xe NMR data. Raman spectroscopic data for $Na_4XeO_6 \cdot 2H_2O$ also support this finding. The Raman spectrum contains six distinct vibrational bands attributable to the XeO_6^{4-} anion [$\nu_1(A_{1g})$, 681 (100) cm^{-1}; $\nu_2(E_g)$, 651 (13) and 641 (8) cm^{-1}; $\nu_4(T_{1u})$, 602 (9) cm^{-1}; $\nu_5(T_{2g})$, 478 (7) 462 (11) cm^{-1}] and two OH stretching bands at 3059 (2) and 2951 (<1) cm^{-1}. The appearance of the moderately intense $\nu_4(T_{1u})$ band at 602 cm^{-1}, which is formally Raman-inactive but infrared-active, and splittings of the degenerate $\nu_2(E_g)$ and $\nu_5(T_{2g})$ modes are consistent with a XeO_6^{4-} anion distorted from O_h symmetry in the dihydrate. The two OH stretching bands of the water molecules of hydration appear at considerably lower frequencies than those for gaseous water (3756 and 3657 cm^{-1}),[69] indicating strong hydrogen bonding.

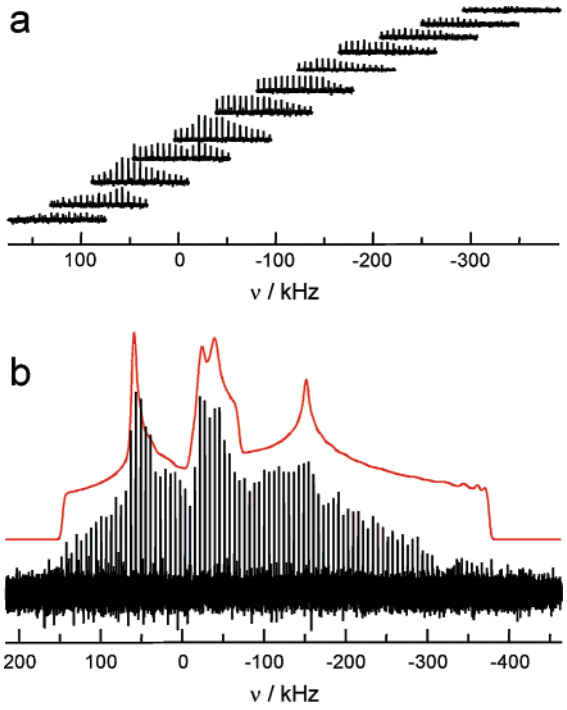

Figure 4. (a) Selected ^{131}Xe NMR spectra of a stationary sample of $Na_4XeO_6 \cdot 2H_2O$ acquired using the stepped-frequency technique at 11.75 T; $\nu(^{131}Xe) = 41.2136$ MHz. Each spectrum is the sum of 142 848 scans and was acquired using a 1-s pulse delay and $\nu_{QCPMG} = 6055$ Hz. (b) A total of 15 subspectra were superimposed to give the "skyline" projection of the ^{131}Xe NMR spectrum (bottom trace). The simulated ^{131}Xe NMR spectrum (top trace) has been calculated using the parameters given in Table 1. The broad component is attributed to $Na_4XeO_6 \cdot 2H_2O$, and the narrow, central component is the sum of two sites attributed to two unknown hydrates of Na_4XeO_6.

The solid-state ^{131}Xe NMR spectrum of $Na_4XeO_6 \cdot 2H_2O$ clearly demonstrates the highly sensitive nature of the xenon EFG tensor to small changes in the local xenon environment relative to the xenon shielding tensor. While the span of the ^{129}Xe shielding tensor is only 95 ppm (3.9 kHz), the ^{131}Xe second-order quadrupolar line shape is much broader (500

(66) The demonstration version of the nonlinear regression program is available at www.nlreg.com.
(67) Alemany, L. B.; Grant, D. M.; Pugmire, R. J.; Alger, T. D.; Zilm, K. W. *J. Am. Chem. Soc.* **1983**, *105*, 2133−2141.
(68) Blümich, B.; Ziessow, D. *J. Magn. Reson.* **1982**, *49*, 151−154.
(69) Benedict, W. S.; Gailar, N.; Plyler, E. K. *J. Chem. Phys.* **1956**, *24*, 1139−1165.

kHz), a consequence of the large nuclear ^{131}Xe quadrupole moment, which amplifies structural distortions in XeO_6^{4-}. The ^{131}Xe NMR line shape is unusual and does not represent a characteristic second-order quadrupolar pattern. The span of the ^{129}Xe shielding tensor is small relative to the second-order quadrupolar interaction and therefore has been neglected in the line-shape analysis. Thus, it is reasonable to assume that the impurity hydrate phases previously observed in the ^{129}Xe NMR spectrum at $\delta_{iso} = -700$ and -743 ppm make significant contributions to the ^{131}Xe NMR spectrum. The narrow component, observed near the center of the ^{131}Xe pattern in Figure 4b, is attributed to the two impurity hydrate phases, and the broad peak is attributed to the major component, $Na_4XeO_6 \cdot 2H_2O$. The simulated spectrum, also shown in Figure 4b, has been calculated using three sites with percent contributions of 90:5:5 for $Na_4XeO_6 \cdot 2H_2O$ and the two minor components, respectively. The contributions from the impurity hydrate phases to the ^{131}Xe spectrum are significant because their C_Q values are much smaller relative to those for $Na_4XeO_6 \cdot 2H_2O$. Acquisition of the ^{131}Xe NMR spectrum at a single applied magnetic field prevents a more definitive interpretation of the results for $Na_4XeO_6 \cdot 2H_2O$ and the unknown phases.

The solid-state ^{131}Xe NMR spectra of Na_4XeO_6 and $Na_4XeO_6 \cdot 2H_2O$ demonstrate the sensitivity of the xenon EFG tensor to small changes in the xenon environment. Upon absorption of two water molecules, the symmetry of the XeO_6^{4-} anion is slightly reduced from O_h symmetry, as evidenced by the increase in Ω from 0 to nearly 100 ppm in the solid-state ^{129}Xe NMR spectra. Moreover, the observed $C_Q(^{131}Xe)$ increases from 0 to $\sim$11 MHz, corresponding to ^{131}Xe NMR line widths of 1200 and 500 000 Hz, respectively. From an experimental point of view, the broadening that arises from the second-order quadrupolar interaction is disadvantageous, resulting in ^{131}Xe NMR line shapes that are exceedingly broad and time-consuming to acquire, placing strict limitations on the types of molecules that can presently be successfully examined by solid-state ^{131}Xe NMR spectroscopy. Considering that $C_Q(^{131}Xe)$ values ranging from $\sim$0 to -369.50 MHz[39] have been reported, solid-state ^{131}Xe NMR studies will be useful for examining chemically bound xenon species in which ^{131}Xe is in an environment where the EFGs at xenon are close to zero.

Conclusions

The present study represents an interesting case where solid-state structural information may be gained in the absence of crystal structure data through measurement of the xenon shielding and EFG tensors. The isotropic ^{129}Xe and ^{131}Xe NMR peaks for anhydrous Na_4XeO_6 indicate O_h symmetry, and the Lorentzian ^{129}Xe NMR line shape suggests rapid reorientation of the XeO_6^{4-} anion in the solid state. For $Na_4XeO_6 \cdot 2H_2O$, distortions in the local xenon environment from O_h symmetry have been detected by measuring the xenon magnetic shielding tensor, which is nearly axially symmetric and spans 95 ± 5 ppm, and the EFG tensor, which yields a large ^{131}Xe quadrupolar coupling constant, 10.8 ± 0.5 MHz. Our ^{131}Xe NMR results demonstrate that the ^{131}Xe quadrupolar interaction is highly sensitive to small changes in the local xenon environment. This is a serious drawback in the study of chemically bound xenon species in the solid state, rendering acquisition of ^{131}Xe NMR spectra for species having low-symmetry xenon environments impractical at this time. In contrast, solid-state ^{129}Xe NMR spectroscopic studies are considerably more promising in that both MAS and stationary samples can be studied with relative ease and in reasonable experimental time frames and with no impractical restrictions on the external magnetic field strength.

Experimental Section

Synthesis and Structural Characterization of Sodium Perxenates. A sodium perxenate salt of unknown degree of hydration, $Na_4XeO_6 \cdot xH_2O$, was prepared following a modification of the published synthetic procedure.[14,70] Powder X-ray diffraction (XRD) and thermal gravimetric analysis were used to determine the degree of sample hydration. In addition, the observed XRD pattern for $Na_4XeO_6 \cdot xH_2O$ was compared with the XRD patterns calculated from the single-crystal X-ray structures of $Na_4XeO_6 \cdot 6H_2O$[18] and $Na_4XeO_6 \cdot 8H_2O$.[16] The lack of agreement between either of the calculated XRD patterns and the experimentally determined XRD pattern indicated that the sample was either another hydrate or the anhydrous salt. Subsequent solid-state ^1H NMR experiments confirmed the presence of water, eliminating the anhydrous salt as a possible candidate. Thermal gravimetric analyses indicated that there were approximately two water molecules present, suggesting that the sample is $Na_4XeO_6 \cdot 2H_2O$.

To obtain anhydrous Na_4XeO_6, the sample was heated under dynamic vacuum at 100 °C for 10 h. The absence of water in the sample was confirmed by solid-state ^1H NMR spectroscopy. Raman spectroscopy was used to characterize both sodium perxenate salts, $Na_4XeO_6 \cdot xH_2O$ ($x = 0$, 2) (see the Results and Discussion and Raman Spectroscopy sections).

Solid-State $^{129/131}Xe$ NMR Spectroscopy. The primary NMR reference for $^{129/131}Xe$ NMR spectra, neat $XeOF_4$(l) at 24 °C,[3,27] is not readily available. An alternative $^{129/131}Xe$ NMR reference is xenon gas; however, the $^{129/131}Xe$ chemical shifts are both temperature- and pressure-dependent, making xenon gas a less than ideal reference. The frequency ratio scale has been employed in the present work and is highly recommended for referencing ^{129}Xe NMR spectra, as previously described.[71] This method enables ^{129}Xe NMR spectra to be referenced with respect to the primary Xe NMR reference, $XeOF_4$ [neat liquid; 24 °C, $\Xi(^{129}Xe) = 27\,810\,184$ Hz] without direct use of the primary reference. The ^{131}Xe NMR resonance of $XeOF_4$(l) cannot be observed as a consequence of rapid quadrupolar relaxation; thus, ^{131}Xe NMR spectra of the perxenate salts were indirectly referenced to $XeOF_4$(l) using the isotropic ^{129}Xe chemical shifts of XeO_6^{4-}, which ignores the small primary $^{129/131}Xe$ isotope effect. All solid-state $^{129/131}Xe$ NMR spectra were simulated using WSOLIDS[72] and/or SIMPSON.[73]

Na_4XeO_6. Solid-state $^{129/131}Xe$ NMR spectra of Na_4XeO_6 were acquired on a Bruker Avance NMR spectrometer operating at

(70) Jaselskis, B.; Spittler, T. M.; Huston, J. L. *J. Am. Chem. Soc.* **1966**, *88*, 2149−2150.
(71) Schumacher, G. A.; Schrobilgen, G. J. *Inorg. Chem.* **1984**, *23*, 2923−2929.
(72) Eichele, K.; Wasylishen, R. E. *WSOLIDS NMR Simulation Package*, version 1.17.26; 2000.
(73) Bak, M.; Rasmussen, J. T.; Nielsen, N. C. *J. Magn. Reson.* **2000**, *147*, 296−330.

^{129}Xe and ^{131}Xe frequencies of 139.0314 and 41.2136 MHz, respectively ($B_0 = 11.75$ T). Samples of Na_4XeO_6 were powdered and packed into a 7-mm ZrO_2 rotor, which was 75% full. Because the rotor was only partially filled, we were unable to safely carry out $^{129/131}$Xe NMR experiments on MAS samples of anhydrous Na_4XeO_6; hence, only experiments on stationary samples were performed. Experiments were carried out using a double-resonance probe. To ensure the hygroscopic sample did not absorb water, nitrogen gas was continuously flowed over the anhydrous sample through the bearing-gas line to the probe.

For ^{129}Xe NMR experiments, a simple one-pulse sequence was used with a sweep width of 100 kHz, an acquisition time of 10.2 ms, a $\pi/2$ pulse width of 2.00 μs, and pulse delays varying from 2 to 600 s. To estimate $T_1(^{129}\text{Xe})$ for Na_4XeO_6, the progressive saturation technique[64] was employed, and four dummy pulses were applied before the acquisition of 16 scans to ensure that a steady state was established and pulse delays ranging from 2 to 800 s were used. The data were fit to $S_\tau = S_\infty[1 - \exp(-\tau/T_1)]$,[74] where S_τ and S_∞ are the peak intensities after time τ and the time required for the sample to fully relax, respectively, and τ is the time between pulses.

For ^{131}Xe NMR experiments, the pulse width was calibrated using the ^{37}Cl NMR resonance from a solid sample of KCl at $B_0 = 11.75$ T. The frequencies of ^{37}Cl in KCl and ^{131}Xe in $Na_4XeO_6{\cdot}2H_2O$ are 40.8033 and 41.2136 MHz, respectively. Solid-state ^{131}Xe NMR experiments on anhydrous Na_4XeO_6 were carried out using a spin-echo or QCPMG[75,76] sequence. A selective $\pi/2$ pulse width of 2.00 μs and a pulse delay of 1.0 s were used. For the spin-echo (QCPMG) experiment, an acquisition time of 13.27 (86.4) ms and a sweep width of 100 (50) kHz were used. For the ^{131}Xe QCPMG experiment, a spikelet spacing of 200 Hz and π pulse repetition of 22 were used.[7]

$Na_4XeO_6{\cdot}2H_2O$. A 4-mm triple-resonance probe was used to acquire ^{129}Xe NMR spectra of stationary and MAS samples of $Na_4XeO_6{\cdot}2H_2O$ using either standard one-pulse or $^1\text{H} \rightarrow {}^{129}\text{Xe}$ CP methods. Proton decoupling, $(\gamma B_1/2\pi) = 60$ kHz, was used in all experiments. The magic angle was set by maximizing the number of rotational echoes in the ^{79}Br NMR free-induction decay of solid KBr. To calibrate the $\pi/2$ pulse for ^{129}Xe one-pulse experiments, the ^{13}C NMR resonance of adamantane was used; the respective ^{13}C and ^{129}Xe frequencies for adamantane and sodium perxenate at 11.75 T are 125.8027 and 139.0314 MHz, respectively. A $\pi/4$ pulse angle, pulse delays ranging from 30 to 600 s, a sweep width of 100 kHz, and an acquisition time of 10.2 ms were used to acquire ^{129}Xe NMR spectra of stationary and MAS samples of $Na_4XeO_6{\cdot}2H_2O$. For $^1\text{H} \rightarrow {}^{129}\text{Xe}$ CP experiments, acquisition parameters were optimized on the $Na_4XeO_6{\cdot}2H_2O$ sample at spinning rates ranging from 1342 to 6000 Hz. A ^{1}H $\pi/2$ pulse width of 4.25 μs, a pulse delay of 2 s, and contact times of 7−9 ms were used for ^{129}Xe CP/MAS experiments. To determine the $^1\text{H}-{}^{129}\text{Xe}$ CP time, $T_{^1\text{H},^{129}\text{Xe}}$, and the ^{1}H T_1 relaxation time in the rotating frame, $T_{1\rho}(^1\text{H})$, for $Na_4XeO_6{\cdot}2H_2O$, a series of ^{129}Xe CP/MAS experiments were performed by monitoring the ^{129}Xe NMR peak intensity as a function of the contact time.

A 7-mm double-resonance probe was used to acquire stepped-frequency[77] $^{131}\text{Xe}\{^1\text{H}\}$ QCPMG NMR spectra of a stationary sample of $Na_4XeO_6{\cdot}2H_2O$. A total of 15 subspectra were collected, whereby the transmitter or carrier frequency, ν_c, was adjusted in increments of 42 kHz. Prior to each experiment, the tune and match of the ^{1}H and ^{131}Xe channels were meticulously adjusted. Selective $\pi/2$ and π pulses were found to be 2.75 and 5.5 μs, respectively, for the ^{131}Xe channel and an optimized ^{1}H $\pi/2$ decoupling pulse of 13.0 μs was used. A sweep width of 100 kHz, an acquisition time of 13.3 ms, and a pulse delay of 1 s were used to acquire 142 848 scans. The QCPMG π pulse train was repeated 80 times using delays of 100 μs before and after each π pulse, and τ_a was set to 80 μs, which corresponds to a separation between spikes in the NMR spectrum, ν_{QCPMG}, of approximately 6.0 kHz. The skyline projection method[68] was used to process the stepped-frequency spectra. This method superimposes the various subspectra, rather than co-adding them, to produce a single spectrum that represents the ^{131}Xe NMR line shape of $Na_4XeO_6{\cdot}2H_2O$.

Raman Spectroscopy. The Raman spectra of Na_4XeO_6 and $Na_4XeO_6{\cdot}2H_2O$ were recorded on a Bruker RFS 100 FT Raman spectrometer with a quartz beam splitter, a liquid-nitrogen-cooled germanium detector, and a low-temperature accessory. The back-scattered (180°) radiation was sampled. The actual usable Stokes range was 50−3500 cm^{-1} with a spectral resolution of 2 cm^{-1}. The 1064-nm line of an Nd:YAG laser was used for excitation of the sample. The low-temperature (−100 °C) spectra of Na_4XeO_6 and $Na_4XeO_6{\cdot}2H_2O$ were recorded on powdered samples sealed in melting point capillaries using laser powers of 300 and 250 mW, respectively.

Thermal Gravimetric Analysis. Data were collected on a Perkin-Elmer Pyris I thermal gravimetric analyzer at atmospheric pressure under a flow of nitrogen gas. Two determinations were carried out for temperature ranges of 20−200 and 20−350 °C at a rate of 5 °C min^{-1}. Loss of two water molecules occurred in an apparent stepwise fashion at 80−88 and 98−124 °C.

Powder XRD. The powder XRD patterns of $Na_4XeO_6{\cdot}2H_2O$ were recorded on an Inel Equinox 3000 powder diffractometer equipped with a Cu Kα radiation source ($\lambda = 1.540\,56$ Å), using a voltage of 40 kV and a current of 20 mA, and a CPS 120 detector. Data were collected for 2θ angles varying from 5 to 100°.

Acknowledgment. The authors thank the members of the solid-state NMR group at the University of Alberta for interesting discussions on this research and Prof. David Bryce for his efforts during the early stages of this project. R.E.W. is a Canada Research Chair in physical chemistry. We thank the Natural Sciences and Engineering Research Council of Canada (R.E.W., M.G., and G.J.S.), the Alberta Ingenuity Fund (M.A.M.F. and R.E.W.), and the University of Alberta (R.E.W. and M.A.M.F.) for financial support.

IC0624524

(74) Martin, M. L.; Delpuech, J.-J.; Martin, G. J. *Practical NMR Spectroscopy*; Heyden: London, 1979; Chapter 7, p 250.
(75) Cheng, J. T.; Ellis, P. D. *J. Phys. Chem.* **1989**, *93*, 2549−2555.
(76) Larsen, F. H.; Skibsted, J.; Jakobsen, H. J.; Nielsen, N. C. *J. Am. Chem. Soc.* **2000**, *122*, 7080−7086.
(77) Kennedy, M. A.; Vold, R. L.; Vold, R. R. *J. Magn. Reson.* **1991**, *92*, 320−331.